Nuclear spin-lattice relaxation rate in disordered paramagnetic diluted magnetic semiconductors

Huu-Nha Nguyen [1], Minh-Tien Tran,[2] and Van-Nham Phan [3,4,*]

[1]*Department of Theoretical Physics, VNUHCM-University of Science, 227 Nguyen Van Cu, Ho Chi Minh City 700000, Vietnam*
[2]*Institute of Physics, Vietnam Academy of Science and Technology, 10 Dao Tan, Hanoi 10072, Vietnam*
[3]*Institute of Research and Development, Duy Tan University, 3 Quang Trung, Danang 550000, Vietnam*
[4]*Faculty of Natural Sciences, Duy Tan University, 3 Quang Trung, Danang 550000, Vietnam*

Nuclear spin-lattice relaxation signatures in paramagnetic diluted magnetic semiconductors involving magnetic disorder are examined. By utilizing the dynamical mean-field theory for the Kondo lattice model with disorder potential, in the infinite-dimensional limit, we have derived a set of self-consistent equations to enable the numerical evaluation of the single-particle Green's function and its self-energy. The local dynamical spin susceptibility function and then the nuclear spin-lattice relaxation rate is evaluated in terms of the single-particle Green's function. Our numerical results reveal the spin fluctuations, evidenced by the sharp peak appearing at a low frequency in the spin dynamical susceptibility function, become dominant in the case of large magnetic coupling and high magnetic impurity density with temperatures close to the paramagnetic-ferromagnetic transition. In that situation, the nuclear spin-lattice relaxation divided by temperature obeys the Curie law that attributes the formation of the coherent magnetic bound states or the magnons in the paramagnetic state. Sufficiently large intensity of the magnetic disorder or the thermal fluctuations might deplete all of the bound states and then the system would settle in the normal metallic state expressing the Korringa mechanism or the nematic instability. Our observations thus have underlined the significance of the magnetic coupling and the magnetic disorder in determining the spin-lattice relaxation processes in DMSs and highlighted the advantage of the dynamical mean-field theory in studying the spin dynamics in a doped magnetic system.

I. INTRODUCTION

The dynamical scenario of nuclear spin induced by surrounding electrons is always one of the most essential issues stimulating much interest in a strongly correlated electron system. In a nonmagnetic metal or semiconductor, the nuclear spin might be relaxed due to its hyperfine interaction with the surrounding electrons following the Korringa mechanism [1,2]. In a strongly correlated electron system, besides the hyperfine interaction, electrons might strongly correlate with nuclei, the Korringa law generally must be deviated. One of the most prospective schedules to check the Korringa law in a strongly correlated electron system is considering the nuclear spin relaxation in a diluted magnetic semiconductor (DMS) where a slight amount of magnetic ions are doped in a semiconducting host [3,4]. Due to a light doping of magnetic ions, a small localized impurity band appears beside the main band of the host semiconductor. In the case of the Fermi level located in the impurity band, strong correlations between carrier spins and local magnetic moments might release and establish magnetic fluctuations in the systems. The DMS thus plays a dual role of magnetic and semiconducting materials, that might open various potential applications in future spintronics, where the integration of data processing and magnetic storage are incorporated into a single chip [3,4].

The nuclear spin relaxation describes the relaxation of a nonequilibrium spin population of nuclei towards equilibrium. Due to the coupling with surrounding electrons, nuclear spin with higher energies might relax to lower levels and transfer energies to the lattices. The spin-lattice relaxation process can be characterized by a relaxation time T_1; that is the time constant it takes for the energy transfer to establish the equilibrium longitudinal nuclear magnetization. The inverse of the spin-lattice relaxation time $1/T_1$ is the so-called relaxation rate quantifying the damping of the nuclear spin precession due to the coupling to the electron spins, one of the useful quantities revealing basic physics of the electron system. In experiments, the nuclear spin-lattice relaxation rate is usually extracted from the nuclear magnetic resonance (NMR) spectroscopy. NMR measurement has proven to be a powerful probe of local spin dynamics in many strongly correlated electron materials [5]. In theory, the nuclear spin-lattice relaxation rate in turn can be evaluated from the imaginary part of the dynamical spin susceptibility of the electron system, measured at the very low Larmor frequency of the nuclear spins [5]. By using the dynamical mean-field theory (DMFT) or spin-wave and random-phase approximation, the spin-lattice relaxation in a single-band Hubbard model has been addressed [5–10]. In all these studies, the spin-lattice relaxation rate reveals the non-Korringa relation in the strongly electronic correlation limits. In the case of large magnetic coupling, DMS is also one of the strongly correlated electron systems [3,4,11], using DMFT thus is an applicable way to examine the spin-lattice relaxation process in DMSs.

In a dirty metal, one has found that randomness disorder significantly enhances the nuclear spin-lattice relaxation

*Corresponding author: phanvannham@duytan.edu.vn

rates [12]. The observation of Knight shift and NMR relaxation for diluted nonmagnetic alloys has manifested that marked property [13,14]. The disorder thus plays an important impact in the signatures of the nuclear spin-relaxation process in doping system [12]. In DMSs, due to the magnetic doping in the semiconducting host, for instance, doping Mn^{2+} in GaAs, magnetic disorder naturally arises from the random magnetic dopants [11,15–18]. Even in an ideal annealed (Ga,Mn)As sample in which only Ga positions are substituted by Mn ions, randomness in the Mn microstructure also leads to both Coulomb and spin-dependent exchange potential scattering, in some situations, the Coulomb scattering even dominates over the exchange potential scattering [11]. In this sense, the Coulomb scattering or the randomness disorder is actually important near the onset of ferromagnetism at low Mn density [11]. Discussing the nuclear spin-lattice relaxation in DMSs induced by the disorder thus is essential and more practical in comparison with experimental observations. Without the disorder, the nuclear spin-lattice relaxation in DMSs has been recently examined in the framework of the DMFT employed to the Kondo lattice model [19]. The Kondo lattice model here has been proven to be a consistent microscopic model used to investigate the magnetic properties in DMSs [11] and its results have revealed that the nuclear spin-lattice relaxation in DMSs obeys the Korringa rule in the range of large temperature or small magnetic coupling. In the present paper, an additional term describing the disorder in DMSs is involved in the Kondo lattice model as a kind of diagonal disorder. That kind of disorder has been intensively studied in the literature by DMFT [20–24]. Note here that the DMFT has proven as a prevailing method dealing with strongly correlated electron systems, and gives an exact solution in the limit of infinite-dimensional space [20]. The DMFT has been widely used in studying the magnetic properties in DMSs and in other similar systems [25–28]. In our present paper, the nuclear spin-relaxation rate is evaluated from the imaginary part of the dynamical spin susceptibility measured at the very low Larmor frequency of the nuclear spins. In the infinite-dimensional limit, the dynamical spin susceptibility function can be derived in the Baym-Kadanoff approach [29,30]. In the paramagnetic (PM) state, the imaginary part of the spin dynamical susceptibility function shows a sharp peak at a low frequency in the case of large magnetic coupling with temperatures close to the paramagnetic-ferromagnetic (PM-FM) transition. In that situation, one finds the Curie law of the nuclear spin-lattice relaxation divided by temperature that attributes the formation of the coherent magnetic bound states. Increasing the random magnetic disorder or the thermal fluctuations might suppress the bound state and the spin-lattice relaxation rate releases the Korringa law addressing the Fermi-liquid state and then the nematic instability.

The rest of the paper is organized as follows: Section II outlines a microscopic Hamiltonian describing the electronic correlations in DMSs with diagonal disorder represented in real space. In the infinite-dimensional limit, a set of self-consistent equations in DMFT approximation is briefly derived. In Sec. III we present an analytical solution for the dynamical spin susceptibility function and expression for the nuclear spin-lattice relaxation rate. Section IV shows the numerical results and their discussions. A summary and conclusion are presented in Sec. V.

II. HAMILTONIAN AND DYNAMICAL MEAN-FIELD THEORY

In DMSs, magnetic ions are slightly doped in the semiconducting host, and play a role of an acceptor inducing local magnetic moments and itinerant carriers. To describe the electronic and magnetic properties of the DMSs, it is applicable if one uses the Kondo lattice model [11]. In the real space, the microscopic Hamiltonian of the Kondo lattice model involving a magnetic local disorder can be written as

$$\mathcal{H} = -t \sum_{\langle i,j \rangle \sigma} c_{i\sigma}^{\dagger} c_{j\sigma} + 2J \sum_{i} \alpha_i \mathbf{S}_i \mathbf{s}_i - \sum_{i} (\mu - U\alpha_i) n_i, \quad (1)$$

where the first term describes the carrier hopping written in the tight-binding approximation with $c_{i\sigma}^{\dagger}$ and $c_{i\sigma}$ being respectively the creation and annihilation operators of the spin-σ itinerant carrier at lattice site i. t in the first term indicates the hopping integral that is scaled as $t = t^*/\sqrt{2d}$ for a d-dimensional system [20]. In the calculation below, $t^* = 1$ is chosen as the energy unit. In the second term of Hamiltonian (1), $\mathbf{s}_i = \sum_{\sigma\sigma'} c_{i\sigma}^{\dagger} \boldsymbol{\sigma}_{\sigma\sigma'} c_{i\sigma'}/2$ ($\boldsymbol{\sigma}$ are the Pauli matrices) and $\mathbf{S}_i$ are the spin operators of the itinerant carrier and localized impurity moment at lattice site i, respectively. Here we have included a variable $\alpha_i = 1(0)$ to specify if site i is occupied (unoccupied) by a magnetic ion. If x is the doping fraction, α satisfies a binary distribution function $P(\alpha) = (1-x)\delta(\alpha) + x\delta(1-\alpha)$. In the case of $\alpha_i = 1$ for all i, the Hamiltonian recovers the original Kondo lattice model with magnetic randomness disorder [25]. The second term thus expresses the local magnetic coupling J between the itinerant carrier spin and impurity magnetic moment. To simplify our calculation, the magnetic coupling is considered in the Hund-like coupling, i.e., only z component of the magnetic moments is examined. In this case, the second term in Hamiltonian (1) can be rewritten as $2J \sum_i \alpha_i S_i^z s_i^z$, where $s_i^z = \sum_{\sigma} c_{i\sigma}^{\dagger} \sigma c_{i\sigma}/2$. The Hamiltonian given in Eq. (1) has ignored a direct spin-spin interaction between the localized impurity moments. The interaction might significantly affects the nuclear spin-lattice scenario in DMSs and it will be considered in our forthcoming papers.

The local disorder U due to the magnetic doping is given in the last term of the Hamiltonian (1). In the last term, $n_i = \sum_{\sigma} c_{i\sigma}^{\dagger} c_{i\sigma}$ is the occupation number operator of the itinerant carriers and μ is the chemical potential. The disorder potential is mapped onto the difference in the local potential, which splits energetically in favor of the lattice site with and without magnetic doping. It looks like a binary alloy disorder and can be approximately suitable for a lightly doped material [31,32]. In general, the disorder is site dependent; however, in our paper, we handle the bulk system by approximating to infinite dimensions, thus the disorder can be introduced in average and is considered as a kind of diagonal disorder. The diagonal disorder has been intensively studied in the literature by the DMFT [20–24].

To solve the Hamiltonian given in Eq. (1), in the present paper, we use DMFT, one of the powerful methods investigating a strongly correlated electron system. Unlike the

original mean-field theory, DMFT takes into account the lo-cal quantum fluctuations indicating by the time or frequency dependence of the single-particle Green's function [20]. In the infinite-dimensional system, self-energy of the single-particle Green's function is localized, and depends only on the frequency. The single-particle Green's function of the itinerant carrier thus might read

$$G_\sigma(\mathbf{k}, i\omega_n) = \frac{1}{i\omega_n - \varepsilon(\mathbf{k}) + \mu - \Sigma_\sigma(i\omega_n)}, \qquad (2)$$

where $\varepsilon(\mathbf{k}) = -2t\sum_{i=1}^d \cos k_i$ is the dispersion of the itinerant carriers in the tight-binding approximation, $\omega_n = (2n+1)\pi T$ is the fermion Matsubara frequency at temperature T. Equation (2) is a kind of the Dyson equation with the self-energy $\Sigma_\sigma(i\omega_n)$ depending solely on frequency. In the infinite dimensions, the Green's function is also localized, and reads

$$G_\sigma(i\omega_n) = \frac{1}{N}\sum_{\mathbf{k}} G_\sigma(\mathbf{k}, i\omega_n)$$
$$= \int d\varepsilon \rho(\varepsilon)\frac{1}{i\omega_n - \varepsilon + \mu - \Sigma_\sigma(i\omega_n)}. \qquad (3)$$

Here, $\rho(\varepsilon) = \int d^d k/(2\pi)^d \delta(\varepsilon - \varepsilon_{\mathbf{k}})$ is the noninteracting density states. For the hypercubic lattice case, one finds $\rho(\varepsilon) = \exp(-\varepsilon^2)/\sqrt{\pi}$. The Green's function (3) can also be determined by solving an effective single-site problem. In the imaginary time τ representation, that Green function is

$$G_\sigma(\tau) = -\langle \mathcal{T}_\tau c_\sigma(\tau)c_\sigma^\dagger(0)\rangle_{S_{\text{eff}}}, \qquad (4)$$

where $\mathcal{T}_\tau$ is the time ordering operator and S_{eff} is an action of the effective problem. Based on the Hamiltonian written in Eq. (1), the effective action might be read

$$S_{\text{eff}}(s, \alpha) = -\int_0^\beta d\tau \int_0^\beta d\tau' \sum_\sigma c_\sigma^\dagger(\tau)\mathcal{G}_\sigma^{-1}(\tau - \tau')c_\sigma(\tau')$$
$$+ \int_0^\beta d\tau \sum_\sigma [(Js\sigma + U)\alpha - \mu]c_\sigma^\dagger(\tau)c_\sigma(\tau), \qquad (5)$$

with $\mathcal{G}_\sigma(\tau)$ is the bare Green's function of the Weiss effective medium written in the imaginary time representation and $\beta = 1/T$ with T is temperature. s in Eq. (5) is the z component of the localized magnetic moments. The partition function of the effective problem can be evaluated as

$$\mathcal{Z}_{\text{eff}}(\alpha) = \text{Tr}\int Dc^\dagger Dc\, e^{-S_{\text{eff}}(s,\alpha)}, \qquad (6)$$

where Tr implies the trace taken over all values of s. Using the Fourier transformations $c_\sigma^{(\dagger)}(\tau) = (1/\sqrt{\beta})\sum_n c_{n\sigma}^{(\dagger)}\exp(\pm i\omega_n\tau)$, $\mathcal{G}_\sigma(\tau-\tau') = (1/\beta)\sum_n \mathcal{G}_\sigma(i\omega_n)\exp(-i\omega_n(\tau-\tau'))$, and the Grassmann algebra, one might derive an expression of the partition function

$$\mathcal{Z}_{\text{eff}}(\alpha) = 2\text{Tr}\exp\left\{\sum_{n\sigma}\ln\frac{\mathcal{G}^{-1}(i\omega_n) - (Js + U)\alpha}{i\omega_n}\right\}. \qquad (7)$$

The local single-particle Green's function of the effective problem defined in Eq. (4) can be evaluated from the partition

function. In the Matsubara frequency representation, one has

$$G_\sigma(i\omega_n) = \int d\alpha P(\alpha)\frac{\delta\ln\mathcal{Z}_{\text{eff}}(\alpha)}{\delta\mathcal{G}^{-1}(i\omega_n)}, \qquad (8)$$

and finds an explicit expression of the single-particle Green's function of the effective problem

$$G_\sigma(i\omega_n) = (1-x)\text{Tr}\frac{w_{0s}}{\mathcal{G}^{-1}(i\omega_n)} + x\text{Tr}\frac{w_{1s}}{\mathcal{G}^{-1}(i\omega_n) - Js\sigma - U}, \qquad (9)$$

where $w_{\alpha s}$ ($\alpha = \{0, 1\}$) indicates the weight factors that are the functionals of the Green's function

$$w_{\alpha,s} = \frac{1}{\mathcal{Z}_{\text{eff}}(\alpha)}\exp\sum_{n\sigma}\ln\frac{\mathcal{G}^{-1}(i\omega_n) - (Js + U)\alpha}{i\omega_n}. \qquad (10)$$

As addressed above, $\mathcal{G}^{-1}(i\omega_n)$ plays a role of the Green's function describing the noninteracting Weiss effective medium around the carrier localized at a lattice site. The local Green's function of the itinerant carrier with respect to spin σ thus might be read, following the Dyson's equation

$$G_\sigma(i\omega_n) = \frac{1}{\mathcal{G}_\sigma^{-1}(i\omega_n) - \Sigma_\sigma(i\omega_n)}. \qquad (11)$$

From Eqs. (3), (9), and (11) one finds a set of self-consistent equations permitting us determining numerically the local Green's function and self-energy depending on frequency of the itinerant carriers for a given set of parameters.

III. DYNAMICAL SPIN SUSCEPTIBILITY FUNCTION AND NUCLEAR SPIN-RELAXATION RATE

The nuclear spin-lattice relaxation rate, in the present paper, is analyzied in the signatures of the dynamical spin susceptibility of the carriers. In doing so, the nuclear spin-lattice relaxation rate divided by temperature T is evaluated from the imaginary part of the dynamical spin susceptibility function measured at the very low Larmor frequency of the nuclear spins [5]

$$\frac{1}{T_1 T} = \lim_{\omega_L \to 0}\frac{1}{N}\sum_{\mathbf{q}}|A(\mathbf{q})|^2\frac{\text{Im}\chi^{zz}(\mathbf{q}, \omega_L)}{\omega_L}, \qquad (12)$$

where $\chi^{zz}(\mathbf{q}, \omega)$ is momentum $\mathbf{q}$ dependence of the transverse dynamical spin susceptibility function and ω_L is the Larmor frequency [20]. $A(\mathbf{q})$ in Eq. (12) is a hyperfine interaction. In case that the hyperfine interaction is momentum independent, $1/T_1 T$ can be estimated as the slope of the imaginary part of the local spin susceptibility function $\chi_{\text{loc}}^{zz} = \chi^{zz}(\omega) = (1/N)\sum_{\mathbf{q}}\chi^{zz}(\mathbf{q}, \omega)$ in the zero-frequency limit [7]. To evaluate the nuclear spin-lattice relaxation rate, firstly, we determine the transverse dynamical spin susceptibility function. In the imaginary time representation, one might define

$$\chi_{ij}^{zz}(\tau, \tau') = \langle \mathcal{T}s_i^z(\tau)s_j^z(\tau')\rangle, \qquad (13)$$

where $\mathcal{T}$ is the imaginary time order operator and

$$s_i^z(\tau) = \frac{1}{2}\sum_\sigma c_{i\sigma}^\dagger(\tau)\sigma c_{i\sigma}(\tau) \qquad (14)$$

is time dependence of the z component of the spin operator at lattice site i. Using the Fourier transformation, one might find

the transverse dynamical spin susceptibility function written in momentum and frequency spaces

$$\chi^{zz}(\mathbf{q}, i\omega_l) = \int_0^\beta d\tau e^{i\omega_l \tau} \sum_{ij} e^{i\mathbf{q}(\mathbf{R}_i - \mathbf{R}_j)} \langle \mathcal{T} s_i^z(\tau) s_j^z(0) \rangle, \quad (15)$$

where $\omega_l = 2\pi T l$ is a bosonic Matsubara frequency. Note here that the real frequency ω dependence of the susceptibility in Eq. (12) can be obtained from its Matsubara frequency in Eq. (15) by the analytic continuation $i\omega_n \to \omega + i0^+$ [20]. In the infinite-dimension limit, one might deliver the dynamical spin susceptibility in Eq. (15) expressed as a summation over bubble and ladder diagrams [20]. It results

$$\chi^{zz}(\mathbf{q}, i\omega_l) = \sum_{nn'} \tilde{\chi}_{\mathbf{q}}^{zz}(i\omega_n, i\omega_{n'}; i\omega_l), \quad (16)$$

where

$$\tilde{\chi}_{\mathbf{q}}^{zz}(i\omega_n, i\omega_{n'}; i\omega_l)$$
$$= \tilde{\chi}_{\mathbf{q}}^0(i\omega_n; i\omega_l) \bigg[\delta_{nn'} + \frac{1}{\beta} \sum_{\sigma\sigma'n''} \Gamma^{\sigma\sigma'}(i\omega_n, i\omega_{n''}; i\omega_l) \sigma\sigma'$$
$$\times \tilde{\chi}_{\mathbf{q}}^{zz}(i\omega_{n''}, i\omega_{n'}; i\omega_l) \bigg], \quad (17)$$

where $\tilde{\chi}_{\mathbf{q}}^0(i\omega_n; i\omega_l)$ denotes for the bare susceptibility that is internal momentum summation of the elementary particle-hole bubble contribution,

$$\tilde{\chi}_{\mathbf{q}}^0(i\omega_n; i\omega_l) = -\sum_{\mathbf{k}} G(\mathbf{k}, i\omega_n) G(\mathbf{k} + \mathbf{q}, i\omega_{n+l}). \quad (18)$$

Here we have assumed that the system settles in the homogeneous paramagnetic phase and the spin index is omitted in the Green's function. In the infinite-dimension limit ($d \to \infty$), the momentum dependence of $\tilde{\chi}_{\mathbf{q}}^0(i\omega_n; i\omega_l)$ can be transferred to a single parameter $X = \sum_i \cos q_i / d$ [20,30] given by

$$\tilde{\chi}_{\mathbf{q}}^0(i\omega_n; i\omega_l) = Y \int d\epsilon \rho(\epsilon) \frac{F[Y(X\epsilon - z_{n+l})]}{z_n - \epsilon}, \quad (19)$$

where $Y = -1/\sqrt{1 - X^2}$, $F(x) = \int d\epsilon \rho(\epsilon)/(x - \epsilon)$ is the Hilbert transform of the noninteracting density of states and $z_n = i\omega_n + \mu - \Sigma(i\omega_n)$.

In Eq. (17), $\Gamma^{\sigma\sigma'}(i\omega_n, i\omega_{n'}; i\omega_l)$ plays the role of the local irreducible vertex function that might be evaluated by the Baym-Kadanoff approach [19,29,33,34]. In that scheme, the irreducible vertex function can be produced as the derivative of the self-energy with respect to the Green's function. In the frequency representation, one finds

$$\Gamma^{\sigma\sigma'}(i\omega_n, i\omega_{n'}; i\omega_l) = \frac{1}{T} \frac{\delta \Sigma_\sigma(i\omega_n, i\omega_{n+l})}{\delta G_{\sigma'}(i\omega_{n'}, i\omega_{n'+l})}, \quad (20)$$

where both the Green's function and self-energy are two-frequency dependent. To evaluate the two-frequency dependence of the Green's function, in the DMFT an external magnetic field $h_\sigma(\tau)$ coupling to the itinerant carrier spin is included into the action in Eq. (5). The effective medium Green's function in that reason would be two-time-dependent and from Eq. (9), the two-frequency Green's function

$G_\sigma(i\omega_n, i\omega_m)$ might be written in a matrix form

$$[G_\sigma]_{nm} = \sum_s \int d\alpha P(\alpha) \frac{w_{\alpha,s}}{[\mathcal{G}_\sigma]_{nm}^{-1} - (Js\sigma + U)\alpha}, \quad (21)$$

where the weight factors $w_{\alpha,s}$ are defined in Eq. (10) and $[\mathcal{G}_\sigma]_{nm}^{-1}$ is inverse matrix of the two-frequency effective Green's function. In the first order of the external magnetic field for a single frequency $h_\sigma(i\omega_l)$, the Green's function and self-energy matrices would contain only diagonal ($n = m$) and off-diagonal linearly in $h_\sigma(i\omega_l)$ ($n = m + l$) terms are nonzero [29,30]. The Dyson's equation in Eq. (11) thus might be rewritten in matrix form like

$$\Sigma_\sigma(i\omega_n, i\omega_{n+l}) = [G_\sigma]_{n,n+l}^{-1} - [\mathcal{G}_\sigma]_{n,n+l}^{-1}. \quad (22)$$

Combining Eq. (22) with Eq. (21), one might derive an explicit relation between the two-frequency self-energy and its Green's function as

$$\Sigma_\sigma(i\omega_n, i\omega_{n+l}) = \frac{\Pi_{nl}^\sigma}{\Xi_{nl}^\sigma} G_\sigma(i\omega_n, i\omega_{n+l}), \quad (23)$$

where

$$\Pi_{nl}^\sigma = \frac{\Sigma_\sigma(i\omega_n) - 2U}{2G_\sigma(i\omega_{n+l})} \big[\mathcal{G}_\sigma^{-1}(i\omega_n) + \mathcal{G}_\sigma^{-1}(i\omega_{n+l}) \big]$$
$$- [\Sigma_\sigma(i\omega_{n+l}) - 2U] \big[\mathcal{G}_\sigma^{-1}(i\omega_{n+l}) \big]^2$$
$$+ \frac{A_\sigma + U}{2G_\sigma(i\omega_n)G_\sigma(i\omega_{n+l})} - (U^2 - J^2)\Sigma_\sigma(i\omega_{n+l}), \quad (24)$$

and

$$\Xi_{nl}^\sigma = G_\sigma(i\omega_n) \big\{ \big[\Sigma_\sigma(i\omega_n) - 2U \big] \big[\mathcal{G}_\sigma^{-1}(i\omega_n) + \mathcal{G}_\sigma^{-1}(i\omega_{n+l}) \big]$$
$$+ U^2 - J^2 + \big[\mathcal{G}_\sigma^{-1}(i\omega_{n+l}) \big]^2 \big\} + A_\sigma + U, \quad (25)$$

in which we have denoted

$$A_\sigma = U(1 - x)(w_{0,-1} + w_{0,1}) + J\sigma x(w_{1,-1} - w_{1,1}). \quad (26)$$

Equation (23) gives us a solution of the derivation in Eq. (20) and one finds an analytical expression for the irreducible vertex function

$$\Gamma^{\sigma\sigma'}(i\omega_n, i\omega_{n'}; i\omega_l) = \delta_{\sigma\sigma'}\delta_{nn'} \frac{1}{T} \frac{\Pi_{nl}^\sigma}{\Xi_{nl}^\sigma}, \quad (27)$$

From the simple result in Eq. (27), the correlation function $\tilde{\chi}_{\mathbf{q}}(i\omega_n, i\omega_{n'}; i\omega_l)$ in Eq. (17) and then the dynamical transverse spin susceptibility function in Eq. (16) can be written in a regular expression

$$\chi(\mathbf{q}, i\omega_l) = T \sum_n \frac{1}{\big[\tilde{\chi}_{\mathbf{q}}^0(i\omega_n; i\omega_l) \big]^{-1} - \Gamma_{nl}}, \quad (28)$$

where $\Gamma_{nl} = \sum_\sigma \Pi_{nl}^\sigma / \Xi_{nl}^\sigma$ plays the role of the vertex function. Note here that Π_{nl}^σ and Ξ_{nl}^σ, denoted respectively in Eqs. (24) and (25), depend on the single-fermionic Matsubara frequency Green's function and its self-energy only. Evaluating Γ_{nl} and then the dynamical susceptibility function in Eq. (28) thus become simple by the solutions of the DMFT in the previous section. The nuclear spin-lattice relaxation rate can be straightforwardly determined in the formula of Eq. (12).
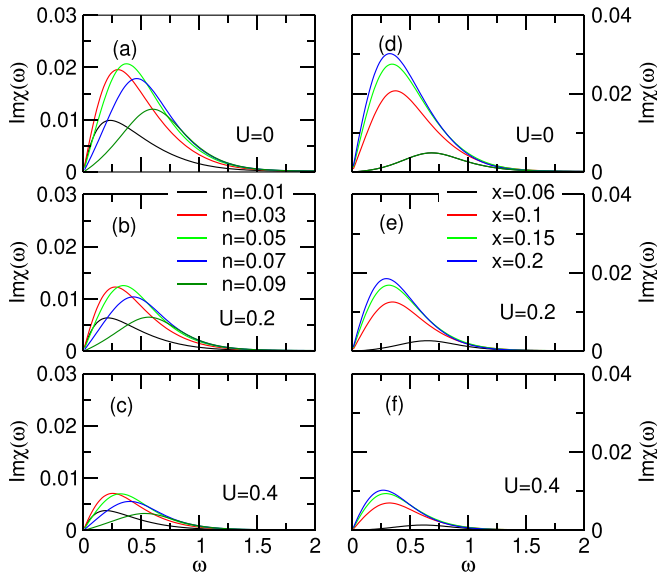
FIG. 1. Imaginary part of the local dynamical spin susceptibility function $\text{Im}\chi(\omega)$ for different disorder strengths U at $J = 4$ and $T = 0.1$ for different carrier densities n with $x = 0.1$ (left panels), and for different magnetic doping x with $n = 0.05$ (right panels).

IV. NUMERICAL RESULTS

In order to find solutions of the local Green's function of the itinerant carriers in Eq. (3) and its respective self-energy, we solve self-consistently the set of equations in Eqs. (3), (9), and (11). To simplify our further calculation, all Matsubara frequencies are transformed to the real frequency by using the analytical continuous $i\omega_n \rightarrow \omega + i0^+$. In that manner, the dynamical spin susceptibility in Eq. (28) can be represented in the real frequency ω, the limitation in Eq. (12) and then the nuclear spin-lattice relaxation rate can be easily evaluated.

Firstly, we discuss the spin fluctuations in the system by analyzing a spectrum of the imaginary part of the local dynamical spin susceptibility function $\text{Im}\chi(\omega)$. In Fig. 1 we show $\text{Im}\chi(\omega)$ for a given large magnetic coupling $J = 4$ by varying the disorder strength U, itinerant carrier densities n, and the magnetic doping x. In the calculation, the temperature $T = 0.1$ is chosen to ensure that the system settles in the PM state. Note here that, in realistic DMSs, for instance (Ga,Mn)As, the lattice constant $a \sim 5.64\,\text{Å}$ and one finds the hopping term $t^* \sim 1.5$ eV, or even in (Ga,Mn)N, $a \sim 4.42$ Å, the hopping term t^* is around 0.5 eV [35]. The magnetic coupling, respectively, evaluated for (Ga,Mn)As is in between 0.89 eV and 3.34 eV, or that with the GaN host in the range 1.85–6.93 eV [35–40]. So in the unit of the hopping term t^*, the range of temperature T and magnetic coupling $2J$ used in the our present calculation are reasonable. For a given set of parameters, all panels show us that the imaginary part of the susceptibility always indicates a single peak at a low frequency ω_0, representing the fluctuations or the magnetic coherent bound states of the local moments even in the PM state. In the absence of the magnetic disorder ($U = 0$), Fig. 1(a) shows that the peak shifts towards a higher frequency as increasing the density of the itinerant carriers for fixed magnetic density $x = 0.1$. The small

values of ω_0 observed at low itinerant carrier density can be explained by an energetical creating of the magnetic bound state once all itinerant carriers enable feeling the magnetic coupling with the local magnetic moments. However, as the carrier density increases, the correlation between carriers and local moments is screened, resulting in a suppressed bound coherence energy or magnetic fluctuations being restrained in the system. Consequently, the peak in the local dynamical spin susceptibility shifts towards the right at a higher frequency. In varying the carrier density, the peak in the susceptibility spectrum gets maximum at $n = 0.05$ corresponding to the half-filled impurity band situation, $n = x/2$. Note here that in the half-filled band case, the critical temperature for the PM-FM transition reaches a maximum for a large magnetic coupling [25,27]. As the temperature is lowered from the PM state, the magnetic fluctuations become reinforced rather than the case in which the impurity band deviates from the half-filled situation. The magnetic coherence thus is most favorable in the half-filled impurity band case. For the fixed value of the magnetic impurity doping, all panels on the left show that once the disorder is switched on the spectrum structure of the susceptibility keeps remained. By increasing the disorder, the potential of the magnetic scattering of the itinerant carriers with majority spin is decreased while that of the minority spin is increased [26,27,41]. As a consequence, taking into account the disorder diminishes the magnetic coherent bound state in the diluted system, that is specified by the suppression of the peak height in the susceptibility spectrum once increasing the disorder strength [see Figs. 1(a)–1(c)].

Once the itinerant carrier density is fixed but the magnetic impurity doping is varied, increasing the magnetic disorder also suppresses the dynamical susceptibility spectrum. Indeed, in Figs. 1(d)–1(f) we address $\text{Im}\chi(\omega)$ for some values of x at given $n = 0.05$ with three different values of the magnetic disorder strength. As increasing the disorder, the height of the $\text{Im}\chi(\omega)$ is depressed corresponding to diminishing the magnetic coherent bound states above the FM critical temperature. At a given itinerant carrier density, increasing the magnetic impurity density generally reinforces the possibility for the magnetic correlations between the itinerant carriers with the localized moments, resulting energetically in the magnetic bound state of the carriers. That scenario has been specified by enlarging height and shifting to the left of the peak in the dynamical susceptibility spectrum shown in the right panels in Fig. 1.

To inspect in more detail the magnetic resonance induced by the presence of the magnetic randomness disorder in Fig. 2, where we present the imaginary part of the local dynamical spin susceptibility function $\text{Im}\chi(\omega)$ for different values of the disorder U by varying the temperature T and magnetic coupling J at $x = 0.1$ and $n = 0.05$. We have to note here that within the range of the set parameters, the system maintains the PM state and the single peak structure in the imaginary part of the local dynamical spin susceptibility function $\text{Im}\chi(\omega)$ remains signifying a magnetic coherence bound state above the critical transition point. For a given large magnetic coupling $J = 4$, all panels in the left of Fig. 2 display the temperature dependence of the $\text{Im}\chi(\omega)$ spectrum for different values of the magnetic randomness disorder. For a fixed randomness disorder, the peak appearing in $\text{Im}\chi(\omega)$ gets sharper
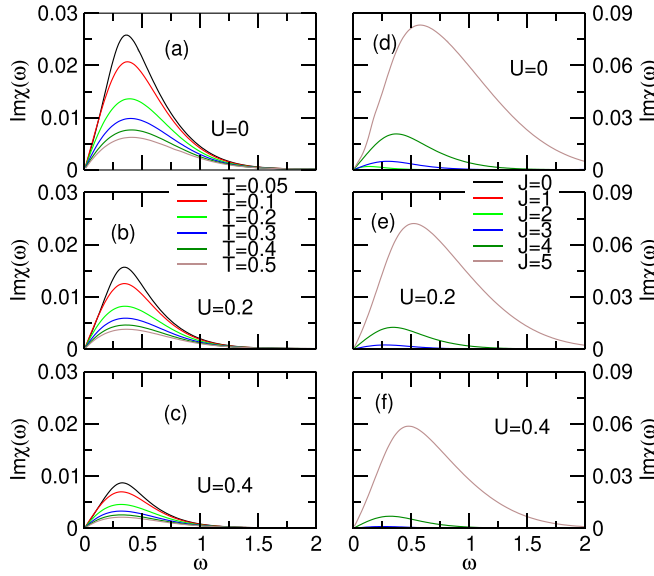
FIG. 2. Imaginary part of the dynamical local spin susceptibility function $\text{Im}\chi(\omega)$ for different disorder strengths U at $x = 0.1$ and $n = 0.05$ for different temperatures T with $J = 4$ (left panels), and for different magnetic coupling J with $T = 0.1$ (right panels).

FIG. 3. $1/T_1T$ as a function of temperature T at given randomness magnetic disorder $U = 0.2$ for carrier doping $n = 0.07$ with some data fits (a) and for different carrier dopings n (b) at $J = 4$ and $x = 0.1$. T_{SF} and T_{FL} in panel (a) indicate the magnetic fluctuation and Fermi-liquid transition temperatures that are addressed in solid red and dashed purple arrows, respectively in the panel (b).

and shifts to the left as decreasing temperature. In the presence of thermal fluctuations, the bound state of the magnetic coherence might be more or less destructed. Indeed, increasing the thermal fluctuations causes a loss of the magnetic bound states between the carrier spins and local moments, the magnetic bound states thus might be destroyed. That evaluation has been indicated in the shifting of the peak towards a higher frequency as increasing temperature. The significant rise of the peak at low frequency in the local dynamical spin susceptibility when the temperature reaches the critical PM-FM transition point, in the meanwhile, demonstrates the strong spin fluctuations attributing the bound state of the magnetic coherence occurring before the FM transition. By switching on the magnetic disorder, the magnetic scattering potential depresses the magnetic coherent bound states. The effect of the magnetic disorder can be signified in the height suppression of the peak in $\text{Im}\chi(\omega)$ as increasing the disorder [see Figs. 2(a)–2(c)].

The effect of the magnetic randomness disorder on the magnetic bound state before the PM-FM transition in DMSs can also be indicated in the left panels of Fig. 2. Indeed, Figs. 2(d)–2(f) has addressed the suppression of the $\text{Im}\chi(\omega)$ by increasing the magnetic disorder U at any given value of the magnetic coupling J for $T = 0.1$, $x = 0.1$, and $n = 0.05$. Once the disorder is fixed, increasing the magnetic coupling rapidly reinforces the $\text{Im}\chi(\omega)$ intensity, especially at low frequency. The identification specifies the significant role of magnetic coupling in establishing the formation of magnetic coherence in the PM state. Increasing the magnetic coupling enlarges the magnetic fluctuations of the carriers with respect to local moments that make to reinforce the bound state of the magnetic coherence. The short-range magnetic bound state thus might be formed in case of sufficiently large magnetic coupling once the temperature reaches the FM-PM transition point [cf. Figs. 2(a)–2(c)].
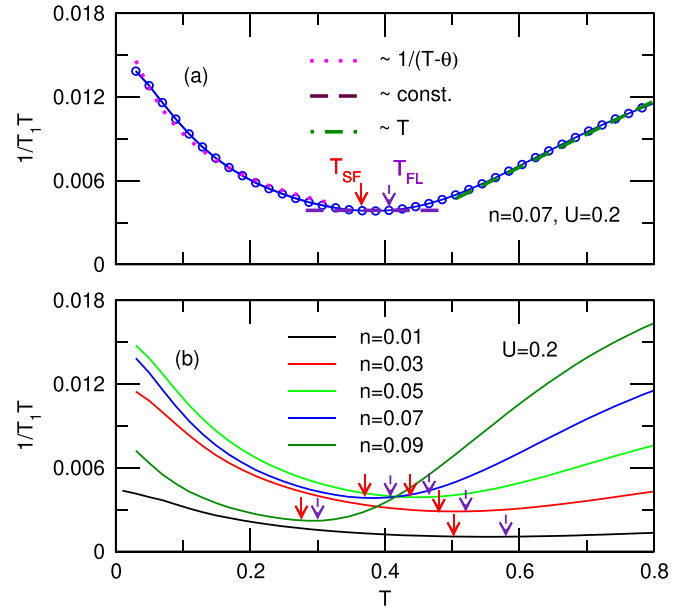
To examine the effect of the magnetic disorder in the spin fluctuations and, more precisely, the nuclear spin-lattice relaxation process, we analyze the spin-relaxation rate divided by temperature $1/T_1T$ as a function of temperature T in Fig. 3 for a given value of magnetic disorder $U = 0.2$ with different carrier densities n at $J = 4$ and $x = 0.1$. In order to inspect explicitly behavior of the nuclear spin-relaxation rate, in Fig. 3(a), we show $1/T_1T$ versus T at a given carrier doping $n = 0.07$ with three different data fits corresponding to three different regions of temperatures. In the large temperature region, $1/T_1T$ decreases linearly by lowering temperatures. This scenario of the $1/T_1T$ versus temperature has been observed in the research of the nuclear spin-lattice relaxation in optimally doped and overdoped iron-based superconductors at large temperatures [42], the system thus stabilizes in a so-called nematic order state [43–45]. The nematic instability relates to rotational symmetry breaking that is a characteristic feature of the normal state from which at lower temperatures the system might stabilize in some ordered state such as superconductivity, magnetism, or even in topological states [43,44]. Recently, the nematicity fluctuations have been specified in some doped magnetic semiconductors [46]. The strong increase of the nuclear spin-lattice relaxation in this region is typically caused by the thermal activation that accelerates the internal motion. The correlation time then decreases under a fast motion due to thermal fluctuations. For temperatures in the range of $T_{SF} < T < T_{FL}$ one finds $1/T_1T$ to be a constant. The temperature independence $1/T_1T$ specifies the Korringa law of the nuclear spin-lattice relaxation, and the system thus settles in the Fermi-liquid state. In this regime, the strong thermal fluctuations suppress the magnetic correlations and the system behaves like conventional metals. At temperatures

$T < T_{SF}$, in contrast, $1/T_1T$ increases as decreasing temperature following the Curie law, $1/T_1T \sim 1/(T - \theta)$. That behavior of the nuclear spin-lattice relaxation rate releases the reinforcing of the spin fluctuations as decreasing temperature toward the PM-FM transition point [42,47,48]. Within this low-temperature range, although the system might seem to attain a metallic state, it may well revert to an unconventional metal state due to the intensification of spin fluctuations. At such a point, the system generates nonuniform magnetization, leading to the formation of the magnetic coherent bound states close to the PM-FM transition.

Relationships of $1/T_1T$ versus T for other carrier densities at the same set of parameters are addressed in Fig. 3(b). In the whole range of the carrier density, one always finds that $1/T_1T$ decreases then gets a constant and finally increases by decreasing temperature, being separated by T_{SF} and T_{FL}. With increasing carrier density, both of these critical temperatures shift to the left. In DMSs, once the impurity band is partly filled, the movement of the carriers through the lattice is driven by the exchange coupling with the localized magnetic moments. The temperature dependence of the relaxation process can be followed from the Korringa mechanism that reflects the flip-flop transitions of nuclear spins and spins of carriers near the Fermi surface and only carriers within k_BT of the Fermi surface can participate in the nuclear relaxation process [49,50]. In this sense, by increasing the temperature, the probability of the carriers fluctuating in the relaxation process is enhanced that in general reinforces the nuclear spin-lattice relaxation rate. This scenario actually happens in case of large temperatures once the magnetic correlations are suppressed. In this range of large temperatures, increasing the carrier density enhances the fluctuating and the nuclear spin-lattice relaxation rate is developed. However, in the case of lower temperatures, the magnetic correlations play a more important role in settling the mobility of the carriers than that of the thermal fluctuations. The nuclear spin-lattice relaxation rate $1/T_1$ and its temperature dividend $1/T_1T$ thus increase as decreasing temperature. Due to the large magnetic coupling, the relaxation rate thus is largest once the impurity band is half-filled [see the green lines in Fig. 3(b)]. Note here that in the half-filled impurity band case, the mobility of the carriers becomes most favored in the case of large magnetic coupling, resulting the promotion of the nuclear spin-lattice relaxation rate. Once the thermal fluctuations become less important, the behavior of the spin-relaxation rate versus carrier density in the low-temperature range once more indicates the spin fluctuation signatures as addressed in Figs. 1(a)–1(c) and in Fig. 3(a) with the formation of the magnetic coherent bound state above the PM-FM transition point. The Curie law in $1/T_1T$ behavior also attributes the magnon processes contributing to the spin-lattice relaxation like in the double-exchange mechanism with Jahn-Teller distortion observed in doped manganites [51]. In the relationships of the spin-relaxation rate, the magnon ascription in our situation is significantly affected by the filling of the impurity band.

To address in detail the complex transitions in the system depending on temperature, we display in Fig. 4 pointing out the phase structure in $T - n$ plane for the parameters settled in Fig. 3. Here, the FM-PM transition temperature is evaluated by the divergence of the static magnetic susceptibility
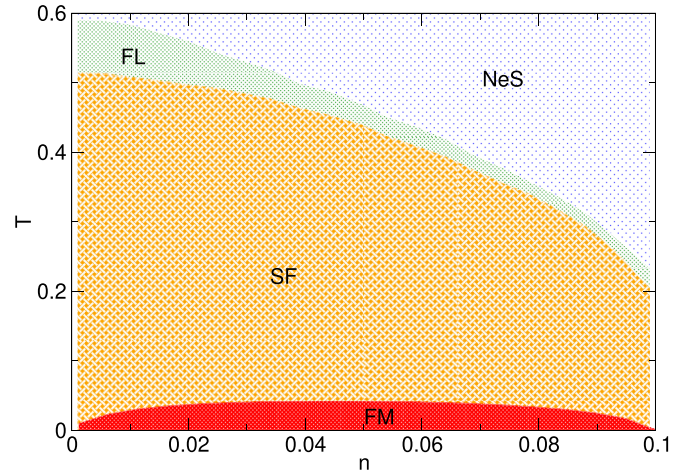

FIG. 4. Phase diagram addressing the instabilities of the nematic state (NeS), Fermi liquid (FL), spin fluctuations (SF), and ferromagnetic state (FM) in the $T - n$ plane for magnetic disorder $U = 0.2$ and magnetic coupling $J = 4$ at magnetic impurity doping $x = 0.1$. The FM transition temperature is evaluated by the divergence of the static magnetic susceptibility function [27].

function [27]. At a given carrier density n, one always finds stability of the FM state at sufficiently low temperatures. With increasing temperature, the thermal fluctuations eliminate the magnetic order and the system settles in the PM state. However, this PM state can be inspected in more detail in the signatures of the nuclear spin-lattice relaxation. Indeed, at temperatures larger than that of the FM-PM transition, firstly one finds the strong spin fluctuations (SF) with respect to the stability of the magnetic bound states. The bound state would be suppressed by reinforcing the thermal fluctuations and the system stabilizes in the Fermi liquid (FL) and then in the nematic state (NeS). The enhancement of the spin fluctuations at low carrier densities can be explained by an energetical creation of the magnetic bound state once all itinerant carriers enable feeling the magnetic coupling with the local magnetic moments. However, as the carrier density increases, the correlation between carriers and local moments is screened, the bound coherence energy thus is suppressed or the magnetic fluctuations are restrained in the system. These properties have also been addressed in the evaluation of the dynamical magnetic susceptibility spectra by varying the carrier density as in the Fig. 1.

To analyze the influence of magnetic coupling on the nuclear spin-lattice relaxation process in the presence of the randomness disorder, we present in Fig. 5 the spin-relaxation rate divided by temperature $1/T_1T$ as a function of temperature T for the half-filled impurity band case ($x = 0.1$ and $n = 0.05$) at different values of the magnetic coupling J and the randomness disorder. For a given set of randomness disorder and magnetic coupling, one always finds three regimes separated by the Fermi-liquid T_{FL} and spin fluctuation T_{SF} critical temperatures. At the large temperature, the thermal fluctuations become dominant and the system settles in the nematic stability and then in the Fermi-liquid states by lowering the temperature to $T < T_{FL}$. At $T < T_{SF}$, $1/T_1T$ follows the Curie law expressing the existence of the mag-
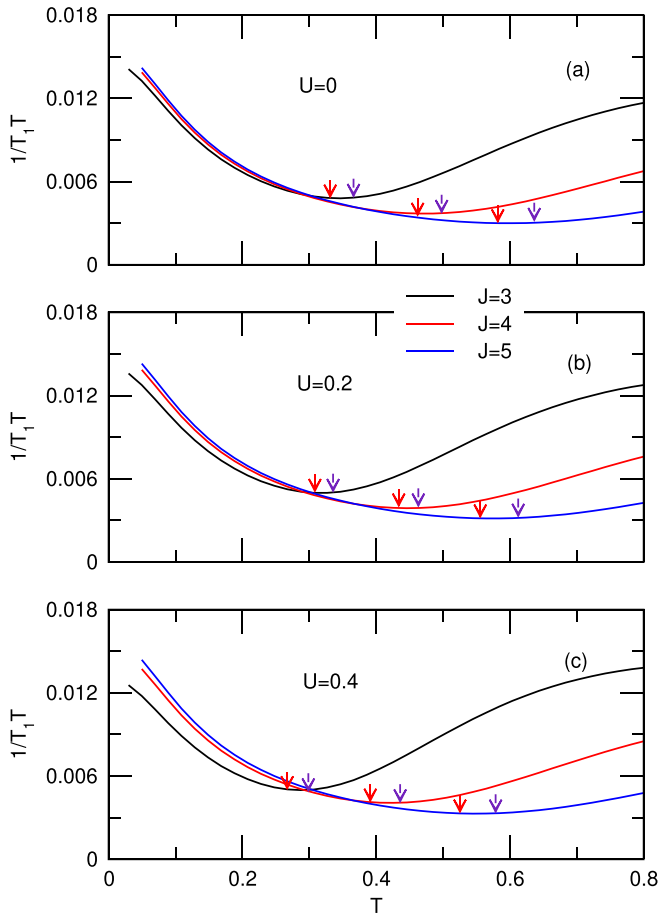
FIG. 5. Nuclear spin-lattice relaxation rate divided by temperature $1/T_1T$ as a function of temperature T for different randomness magnetic disorders U and magnetic couplings J at $x = 0.1$ and $n = 0.05$. The critical temperatures for the spin fluctuation T_{SF} and the Fermi liquid T_{FL} transitions are indicated, respectively, by the solid red and dashed purple arrows.
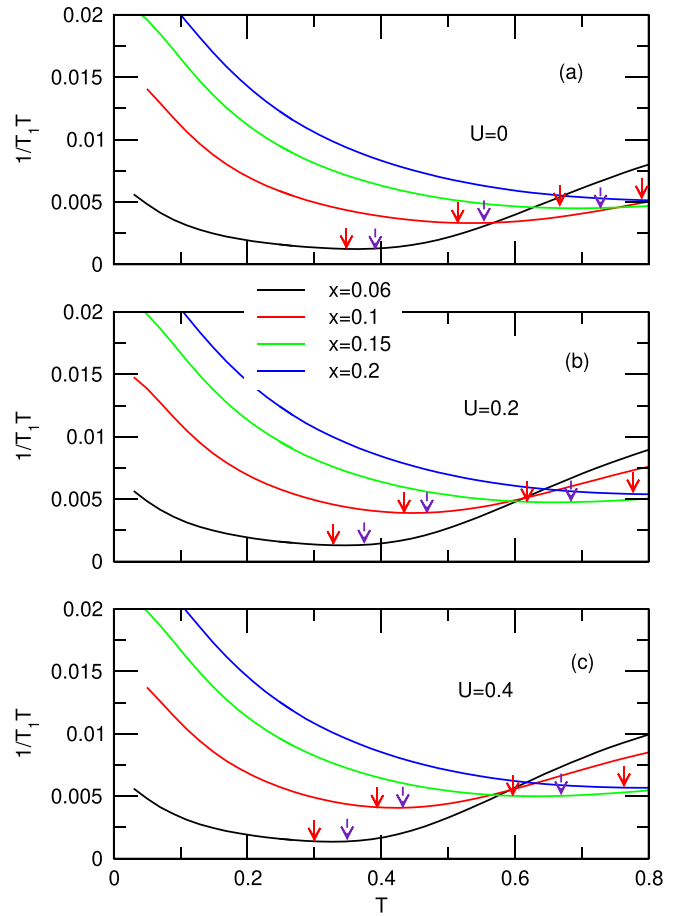
FIG. 6. Nuclear spin-lattice relaxation rate divided by temperature $1/T_1T$ as a function of temperature T for different randomness magnetic disorders U and magnetic doping x at $J = 4$ and $n = 0.05$. The critical temperatures for the magnetic fluctuation T_{SF} and the Fermi liquid T_{FL} transitions are indicated, respectively, by the solid red and dashed purple arrows.

netic fluctuations. That behavior attributes the formation of the magnetic bound state above the PM-FM transition temperature. For a given randomness disorder, T_{SF} shifts to the right with respect to the sustainable magnetic bound state by enlarging magnetic coupling. The magnetic coupling thus plays an important role in reinforcing the FM correlation length in the PM phase, even beyond the PM-FM transition temperature. That signatures have been observed in doped manganites or some other similar materials [52,53]. Increasing the randomness disorder, in one way, suppresses $1/T_1T$ at $T < T_{SF}$ indicating the suppression of the magnetic coherent bound state or the breaking down of the magnon stability due to the presence of the randomness disorder. In contrast, out of the magnetic correlations, i.e., at $T > T_{FL}$, increasing the randomness disorder reinforces the thermal fluctuations and develops the nuclear spin-lattice relaxation rate. Note here that in our model given in Eq. (1), the presence of the randomness disorder excludes the magnetic scattering potential of the majority spin carriers [27]. As a consequence, the critical temperature for the magnetic fluctuation transition T_{SF} (and also T_{FL}) shifts to the left indicating the suppression of the

magnetic coherent bound state by increasing the randomness disorder.

To complete the feature examining the influence of the randomness disorder on the magnetic coherent bound state in DMSs we address in Fig. 6 the dependence of the nuclear spin-lattice relaxation rate divided by temperature $1/T_1T$ versus temperature for different values of randomness disorder U at $J = 4$ and $n = 0.05$ in varying the magnetic doping x. At a given randomness disorder, one always finds the reinforcing of $1/T_1T$ by lowering temperature following the Curie law that addresses the development of the magnetic fluctuations when temperature reaches the critical value of the PM-FM transition. By increasing the magnetic impurity density, the magnetic fluctuation regime broadens to the larger temperature range. Noting here that in the case of the large magnetic coupling, for a given itinerant carrier density increasing the magnetic impurity generally reinforces the possibility for the magnetic correlations between the itinerant carriers with the localized moments, resulting energetically in the magnetic bound state of the carriers. The magnetic bound state thus becomes more stabilized against thermal fluctuations. Of course,

in case of sufficiently high temperature, the large thermal fluctuations would destroy all the magnetic bound states, the system would then settle in the normal metallic state and one finds the Korringa law indicating the Fermi-liquid state at $T_{SF} < T < T_{FL}$ and then the nematic instability at $T > T_{FL}$. For a given magnetic coupling, increasing the randomness disorder also suppresses the magnetic correlations between the itinerant carrier spins and localized moments, specified by the shift to the left with respect to decreasing magnetic fluctuation temperature T_{SF}.

V. CONCLUSIONS

In conclusion, our study has focused on examining the nuclear spin-lattice relaxation process in disordered paramagnetic diluted magnetic semiconductors by utilizing the dynamical mean-field theory for the Kondo lattice model involving localized disorder potential. In the infinite-dimensional limit, we have derived a set of self-consistent equations that allows us to numerically evaluate the single-particle Green's function and its self-energy of the itinerant carriers. These numerical evaluations provide insights into the local dynamical spin susceptibility and then the nuclear spin-lattice relaxation rate of the system. Our findings indicate that, in cases of large magnetic coupling between the itinerant carrier spins and localized moments and temperatures near the paramagnetic-ferromagnetic transition point, the spin fluctuations become dominant addressed by the sharp peak in the spin dynamical susceptibility spectrum appearing at low frequency. The spin fluctuations are suppressed by increasing the magnetic disorder. Signatures of the spin dynamics in the system are also reflected in the properties of the nuclear spin-lattice relaxation process. Indeed, results of the spin-relaxation rate divided by temperature attribute formation of the coherent magnetic bound state or the magnon stability in the paramagnetic phase near the paramagnetic-ferromagnetic transition point, indicated by the breaking down of the Korrigna's law for the temperatures smaller than that critical value of the Fermi liquid to the magnetic fluctuation transition. The coherent magnetic bound state becomes strengthened by increasing the magnetic coupling and magnetic doping density. Increasing the randomness magnetic disorder or thermal fluctuations vice versa suppresses the stability of the bound state. In this case, one finds the Fermi liquid and then the nematic instability when temperature is sufficiently large. Our observations thus have underlined the significance of the magnetic coupling and the magnetic disorders in determining the spin-lattice relaxation processes in DMSs, and highlighted the advantage of the dynamical mean-field theory in studying the spin dynamics in a doped magnetic system.

ACKNOWLEDGMENTS

[1] J. Korringa, Physica **16**, 601 (1950).

[2] M. Kotur, R. I. Dzhioev, K. V. Kavokin, V. L. Korenev, B. R. Namozov, P. E. Pak, and Y. G. Kusrayev, JETP Lett. **99**, 37 (2014).

[3] T. Jungwirth, J. Wunderlich, V. Novák, K. Olejník, B. L. Gallagher, R. P. Campion, K. W. Edmonds, A. W. Rushforth, A. J. Ferguson, and P. Němec, Rev. Mod. Phys. **86**, 855 (2014).

[4] T. Dietl and H. Ohno, Rev. Mod. Phys. **86**, 187 (2014).

[5] T. Pruschke, M. Jarrell, and J. Freericks, Adv. Phys. **44**, 187 (1995).

[6] M. Jarrell and T. Pruschke, Phys. Rev. B **49**, 1458 (1994).

[7] R. Žitko, Ž. Osolin, and P. Jeglič, Phys. Rev. B **91**, 155111 (2015).

[8] X. Chen, J. P. F. LeBlanc, and E. Gull, Nat. Commun. **8**, 14986 (2017).

[9] J. Mußhoff, A. Kiani, and E. Pavarini, Phys. Rev. B **103**, 075136 (2021).

[10] N. Bulut, D. W. Hone, D. J. Scalapino, and N. E. Bickers, Phys. Rev. B **41**, 1797 (1990).

[11] T. Jungwirth, J. Sinova, J. Mašek, J. Kučera, and A. H. MacDonald, Rev. Mod. Phys. **78**, 809 (2006).

[12] B. S. Shastry and E. Abrahams, Phys. Rev. Lett. **72**, 1933 (1994).

[13] A. Narath, CRC Rev. Solid State Sci. **3**, 1 (1972).

[14] D. E. MacLaughlin, C. Tien, W. G. Clark, M. D. Lan, Z. Fisk, J. L. Smith, and H. R. Ott, Phys. Rev. Lett. **53**, 1833 (1984).

[15] A. Kaminski, V. M. Galitski, and S. DasSarma, Phys. Rev. B **70**, 115216 (2004).

[16] M. Berciu and R. N. Bhatt, Phys. Rev. Lett. **87**, 107203 (2001).

[17] A. Kaminski and S. Das Sarma, Phys. Rev. B **68**, 235210 (2003).

[18] V. M. Galitski, A. Kaminski, and S. Das Sarma, Phys. Rev. Lett. **92**, 177203 (2004).

[19] H.-N. Nguyen and V.-N. Phan, Phys. Rev. B **107**, 155113 (2023).

[20] A. Georges, G. Kotliar, W. Krauth, and M. J. Rozenberg, Rev. Mod. Phys. **68**, 13 (1996).

[21] V. Janiš and D. Vollhardt, Phys. Rev. B **46**, 15712 (1992).

[22] R. Strack and D. Vollhardt, Phys. Rev. B **46**, 13852 (1992).

[23] V. Janis, M. Ulmke, and D. Vollhardt, Europhys. Lett. **24**, 287 (1993).

[24] M. Ulmke, V. Janiš, and D. Vollhardt, Phys. Rev. B **51**, 10411 (1995).

[25] A. Chattopadhyay, S. Das Sarma, and A. J. Millis, Phys. Rev. Lett. **87**, 227202 (2001).

[26] E. H. Hwang and S. Das Sarma, Phys. Rev. B **72**, 035210 (2005).

[27] D.-H. Bui, Q.-H. Ninh, H.-N. Nguyen, and V.-N. Phan, Phys. Rev. B **99**, 045123 (2019).

[28] I. D. Marco, P. Thunström, M. I. Katsnelson, J. Sadowski, K. Karlsson, S. Lebègue, J. Kanski, and O. Eriksson, Nat. Commun. **4**, 2645 (2013).

[29] J. K. Freericks and P. Miller, Phys. Rev. B **62**, 10022 (2000).

[30] J. K. Freericks and V. Zlatić, Rev. Mod. Phys. **75**, 1333 (2003).

[31] F. Zhong, J. Dong, and Z. D. Wang, Phys. Rev. B **58**, 15310 (1998).

[32] B. M. Letfulov and J. K. Freericks, Phys. Rev. B **64**, 174409 (2001).

[33] G. Baym and L. P. Kadanoff, Phys. Rev. **124**, 287 (1961).

[34] G. Baym, Phys. Rev. **127**, 1391 (1962).

[35] Y. Yildirim, Ph.D. thesis, Florida State University, 2007.

[36] T. Dietl, H. Ohno, and F. Matsukura, Phys. Rev. B **63**, 195205 (2001).

[37] M. Abolfath, T. Jungwirth, J. Brum, and A. H. MacDonald, Phys. Rev. B **63**, 054418 (2001).

[38] J. Okabayashi, A. Kimura, O. Rader, T. Mizokawa, A. Fujimori, T. Hayashi, and M. Tanaka, Phys. Rev. B **58**, R4211(R) (1998).

[39] F. Matsukura, H. Ohno, A. Shen, and Y. Sugawara, Phys. Rev. B **57**, R2037(R) (1998).

[40] T. Dietl, H. Ohno, F. Matsukura, J. Cibert, and D. Ferrand, Science **287**, 1019 (2000).

[41] V.-N. Phan and H.-N. Nguyen, Phys. Rev. B **102**, 125202 (2020).

[42] F. Hammerath, U. Gräfe, T. Kühne, H. Kühne, P. L. Kuhns, A. P. Reyes, G. Lang, S. Wurmehl, B. Büchner, P. Carretta, and H.-J. Grafe, Phys. Rev. B **88**, 104503 (2013).

[43] R. M. Fernandes, A. V. Chubukov, and J. Schmalian, Nat. Phys. **10**, 97 (2014).

[44] S.-H. Baek, D. V. Efremov, J. M. Ok, J. S. Kim, J. van den Brink, and B. Buechner, Nat. Mater. **14**, 210 (2015).

[45] A. E. Böhmer, T. Arai, F. Hardy, T. Hattori, T. Iye, T. Wolf, H. v. Löhneysen, K. Ishida, and C. Meingast, Phys. Rev. Lett. **114**, 027001 (2015).

[46] Y. Yuan, R. Hübner, M. Birowska, C. Xu, M. Wang, S. Prucnal, R. Jakiela, K. Potzger, R. Böttger, S. Facsko, J. A. Majewski, M. Helm, M. Sawicki, S. Zhou, and T. Dietl, Phys. Rev. Mater. **2**, 114601 (2018).

[47] F. L. Ning, K. Ahilan, T. Imai, A. S. Sefat, M. A. McGuire, B. C. Sales, D. Mandrus, P. Cheng, B. Shen, and H.-H. Wen, Phys. Rev. Lett. **104**, 037001 (2010).

[48] Y. Nakai, T. Iye, S. Kitagawa, K. Ishida, H. Ikeda, S. Kasahara, H. Shishido, T. Shibauchi, Y. Matsuda, and T. Terashima, Phys. Rev. Lett. **105**, 107003 (2010).

[49] M. Kotur, R. I. Dzhioev, M. Vladimirova, B. Jouault, V. L. Korenev, and K. V. Kavokin, Phys. Rev. B **94**, 081201(R) (2016).

[50] M. Vladimirova, S. Cronenberger, D. Scalbert, M. Kotur, R. I. Dzhioev, I. I. Ryzhov, G. G. Kozlov, V. S. Zapasskii, A. Lemaître, and K. V. Kavokin, Phys. Rev. B **95**, 125312 (2017).

[51] M. J. R. Hoch, P. L. Kuhns, W. G. Moulton, A. P. Reyes, M. A. Torija, J. F. Mitchell, and C. Leighton, Phys. Rev. B **75**, 104421 (2007).

[52] V. A. Atsarkin, V. V. Demidov, F. Simon, R. Gaal, Y. Moritomo, K. Conder, A. Jánossy, and L. Forró, J. Magn. Magn. Mater. **258-259**, 256 (2003).

[53] M. S. Seehra and R. P. Gupta, Phys. Rev. B **9**, 197 (1974).